Experimental demonstration of efficient and selective population transfer and qubit distillation in a rare-earth-metal-ion-doped crystal

Lars Rippe, Mattias Nilsson, and Stefan Kröll

Department of Physics, Lund Institute of Technology, P.O. Box 118, SE-22100 Lund, Sweden

Robert Klieber and Dieter Suter

Fachbereich Physik, Universität Dortmund, DE-44221 Dortmund, Germany

In optically controlled quantum computers it may be favorable to address different qubits using light with different frequencies, since the optical diffraction does not then limit the distance between qubits. Using qubits that are close to each other enables qubit-qubit interactions and gate operations that are strong and fast in comparison to qubit-environment interactions and decoherence rates. However, as qubits are addressed in frequency space, great care has to be taken when designing the laser pulses, so that they perform the desired operation on one qubit, without affecting other qubits. Complex hyperbolic secant pulses have theoretically been shown to be excellent for such frequency-addressed quantum computing [I. Roos and K. Molmer, Phys. Rev. A **69**, 022321 (2004)]—e.g., for use in quantum computers based on optical interactions in rare-earth-metal-ion-doped crystals. The optical transition lines of the rare-earth-metal-ions are inhomogeneously broadened and therefore the frequency of the excitation pulses can be used to selectively address qubit ions that are spatially separated by a distance much less than a wavelength. Here, frequency-selective transfer of qubit ions between qubit states using complex hyperbolic secant pulses is experimentally demonstrated. Transfer efficiencies better than 90% were obtained. Using the complex hyperbolic secant pulses it was also possible to create two groups of ions, absorbing at specific frequencies, where 85% of the ions at one of the frequencies was shifted out of resonance with the field when ions in the other frequency group were excited. This procedure of selecting interacting ions, called qubit distillation, was carried out in preparation for two-qubit gate operations in the rare-earth-metal-ion-doped crystals. The techniques for frequency-selective state-to-state transfer developed here may be also useful also for other quantum optics and quantum information experiments in these long-coherence-time solid-state systems.

I. INTRODUCTION

The development of science and technology is continuously bringing the quantum world closer and closer to our daily life. Quantum effects are becoming of increasing importance in the microelectronics and semiconductor industry, and equipment for quantum cryptography is now commercially available [2,3]. As this development proceeds, the need to tailor and control quantum systems will increase, and the experimental realization of quantum computers provides a structured way to develop these techniques. Experiments on quantum computing may be regarded as steps on the way towards the realization of macroscopic superposition states (Schrödinger cats). The numerous practical implementations and theoretical ideas being tested will enable us to master quantum systems to degrees beyond what was generally considered to be possible some years ago. Understanding the limitations and capabilities of the quantum world is an exciting challenge, as is understanding the limitations in controlling quantum systems made out of different types of building blocks and materials.

Quantum computer hardware is presently being developed based on liquids, atoms, or ions or other particles in vacuum, various solids, or all-optical approaches [4]. The level of quantum control obtained so far differs significantly between these systems. The level of control obtained may depend on the physical limitations of the systems, but as the development of new measurement techniques and new technology is a time-consuming process, it may also depend on the extent to which research methods and equipment for controlling the quantum systems already exist. To date, systems with 7 qubits have been demonstrated in NMR on *trans*-crotonic acid molecules [5] and a Cirac-Zoller controlled-NOT (CNOT) quantum gate has been demonstrated on two $^{40}C^+$ ions held in a linear Paul trap [6]. In comparison, the best results for solid-state implementations are rudimentary 2-qubit gates [7,8]. It has been suggested that the extensive manufacturing capabilities developed within the semiconductor and solid-state industry can eventually make it easier to scale quantum computing schemes implemented in solids. However, as a quantum computer operating with 50 qubits will already be able to compete with the best computers available today in solving some classes of problems [4] the importance of a potential larger scalability for solids may be an open question. Regardless of this, quantum system control will become increasingly important in many different solid-state materials in view of the general technology development.

The work presented here concerns qubit formation, qubit control, and qubit-qubit interactions in rare-earth-metal-ion-doped inorganic crystals (RE crystals). RE crystals are used as laser crystals, optical amplifiers, scintillator materials, etc., and, more recently, applications to optical storage and processing and laser stabilization have also emerged [8–10]. These later applications are based on the narrow linewidths
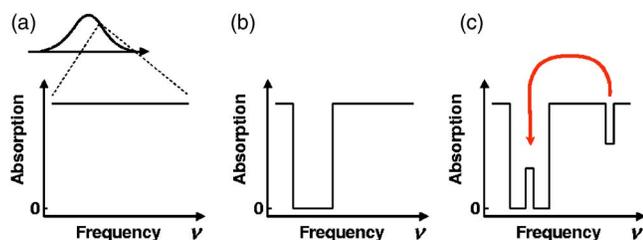
FIG. 1. (Color online) Conceptual illustration of the creation of a peak. (a) When looking at a small part of the inhomogeneous absorption line, the initial absorption appears flat. (b) Scanning the laser frequency back and forth over a region transfers all the ions absorbing within that region to other hyperfine states. (c) A peak of ions absorbing on one hyperfine transition can be transferred back into the pit [27].

[11] and long coherence times that can be obtained for $4f$-$4f$ transitions in RE crystals, at temperatures of a few kelvin. The long coherence times of these transitions have attracted considerable interest in developing quantum computer hardware based on RE crystals [1,8,12–24].

In crystals, the rare-earth-metal-ions may be viewed as a frozen gas. Clearly, for a nonmoving crystal there are no Doppler shifts, but there is a distribution of resonance frequencies for the optical transition, due to variations in the surroundings of the RE ions. The local crystal field shifts the $4f$-$4f$ transition frequencies for the individual ions and these static shifts distribute the absorption frequency of the individual ions across a frequency range of a few GHz, corresponding to 10^5–10^7 homogeneous linewidths. Thus, arbitrarily close-lying ions can be addressed individually using optical pulses, by using light with a specific frequency. Rare-earth-metal-ion hyperfine states may be used as qubit states. Hyperfine-state coherence times of 33 s have recently been observed [25]. As the distance between the RE ions in the crystal can be less than a nanometer, strong ion-ion interactions can be achieved. Ion-ion interactions—e.g., electric-dipole interactions—at these distances may shift the transition frequencies by 10^3–10^6 linewidths, potentially enabling very robust gate operations. This interaction is turned on by promoting one of the interacting ions to an electronically excited state [12].

A major factor preventing the construction of a few-bit quantum computer in RE crystals based on a number of close-lying (and thus also strongly interacting) ions is that a single-ion readout mechanism has not yet been developed. It is reasonably realistic to believe that single-ion readout techniques can be developed as these materials are used as light-sensitive phosphors and, indeed, single-ion readout has now also been demonstrated in rare-earth-metal-ion-doped nanocrystals [26]. However, the complication of single-ion readout can be avoided by boosting the readout signal through the use of quantum computing (QC) schemes where there are many instances of the quantum computer. At each qubit frequency there will be many ions, each belonging to one specific instance, contributing to the signal [21]. This situation is similar to NMR, where the weak signal precludes single-molecule readout. However, there are also many differences between the present scheme and the NMR approach. For

example, the RE crystal ensemble qubits can be prepared in a pure state and the qubit interaction can be turned on and off, which is also demonstrated in the present work.

The experiments described here concern well-defined operations on RE crystal qubits defined in frequency space, where each qubit consists of many quantum systems, which are all in the same pure state and all absorb at nearly the same frequency. In RE-crystal-based QC, the qubits are created by first optically transferring ions absorbing at frequencies in the vicinity of the selected qubit frequency to states not interacting with the field [15,27,28]. The qubit ions then reside within a certain spectral interval on a (near) zero-absorption background (see Fig. 1). High-fidelity quantum gate operations require high fidelity for each qubit operation. This includes well-defined rotations and state transfers of all ions in the qubit illustrated in Fig. 1(c), without exciting ions at other nearby frequencies. Roos and Mølmer [1] have developed a pulse sequence for robust CNOT gate operations on such qubits. The robustness of the scheme stems from the use of complex hyperbolic secant state-to-state transfer pulses (hereafter called sech pulses), commonly used in NMR spectroscopy. The present work confirms the claim by Roos and Mølmer that these pulses are also excellent for high-efficiency state-to-state transfer in the optical region. The successful implementation of efficient operations on the RE crystal qubits and previously demonstrated ground-to-excited-state transfer using sech pulses [18] are important for future high-fidelity quantum gate operations.

The present work also shows that although the narrow homogeneous linewidth is initially buried inside the much wider inhomogeneous line, it is possible to spectrally isolate any selected spectral packet of ions from the rest of the ions in the inhomogeneous profile. Separate operations can then be carried out on the ions in this packet only, such that the favorable coherence properties (narrow linewidths) of the system can be fully used. This can open the way for several applications of these long-coherence-time solid-state systems. For example, a scheme for quantum state storage based on qubit structures such as those investigated here has already been proposed [29].

A long-term goal of the work described in this paper is to implement quantum gates in RE crystals. The next section therefore starts with a brief description of the implementation of a CNOT gate in RE crystals. The qubit preparation, state-to-state transfer and qubit distillation techniques that are described in Sec. II are necessary in order to implement the CNOT operation. Descriptions of the experimental setup and experimental considerations are given in Sec. III. The experimental results on state-to-state transfer and qubit distillation are reported in Secs. IV and V, and the paper ends with a brief summary and outlook.

II. FREQUENCY-SPACE-ADDRESSED QUANTUM COMPUTING USING THE DIPOLE BLOCKADE EFFECT

A. CNOT gate using the dipole blockade effect

We begin by briefly describing how NOT and CNOT operations can be performed in RE crystals by using optical pulses and the dipole blockade effect [12]. Figure 2(a) shows a
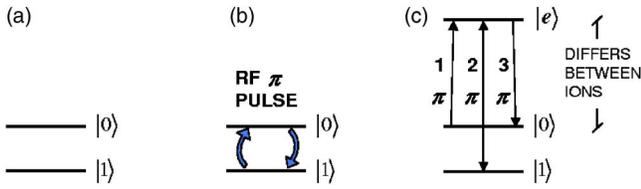
FIG. 2. (Color online) (a) Two of the ground-state hyperfine levels are used as qubit states. (b) In principle a NOT operation can be performed with a radio frequency π pulse. However, this would affect all qubits. (c) Since the optical transition frequency is different for different ions, optical pulses can be used to selectively address one group of ions at a time. The NOT operation between states $|1\rangle$ and $|0\rangle$ now requires three pulses.

simplified energy diagram, where two hyperfine states are used to represent the computational states $|0\rangle$ and $|1\rangle$. A NOT operation between states $|1\rangle$ and $|0\rangle$ could, in principle, be performed with a simple rf π pulse which switches the probability amplitudes between states $|1\rangle$ and $|0\rangle$, as depicted in Fig. 2(b). However, for the RE crystal systems used here the separations between states $|1\rangle$ and $|0\rangle$ are the same for all qubits and such an rf pulse would therefore not be qubit selective. However, as was described in the previous section, the optical transition frequency is different for different qubits and it is therefore possible to carry out qubit-selective operations using optical pulses. These optical pulses are applied to qubits such as those depicted in Fig. 1(c). For example, the NOT gate requires three pulses, as depicted in Fig. 2(c), where $|e\rangle$ denotes an initially empty, optically excited state. The first pulse acts on the state $\alpha|1\rangle + \beta|0\rangle$, performing the operation $\alpha|1\rangle + \beta|0\rangle \rightarrow \alpha|1\rangle + \beta|e\rangle$. The second π pulse performs a NOT operation between states $|1\rangle$ and $|e\rangle$, giving $\alpha|1\rangle + \beta|e\rangle \rightarrow \alpha|e\rangle + \beta|1\rangle$, and the third pulse gives $\alpha|e\rangle + \beta|1\rangle \rightarrow \alpha|0\rangle + \beta|1\rangle$. In order to perform computations, multiqubit gates are necessary. One example is the CNOT gate, where the NOT operation on a target ion only occurs if the control ion is in state $|1\rangle$, and nothing happens if the control ion is in state $|0\rangle$. Below, we give a description of the dipole blockade effect, followed by an implementation of the CNOT operation utilizing this effect.

The mechanism for interaction between qubits, represented by rare-earth-metal ion, is the interaction between static dipole moments of the ions, which causes a shift of the energy levels. Ions in noncentrosymmetric sites in crystals can have a permanent dipole moment, which is caused by a mixing of electronic states with different parity and which is in general different in the ground state and the optically excited state [30,31]. The electric field created by the dipole moment of one ion will affect all nearby ions and cause a Stark shift of their optical transition frequencies. If an ion is excited, its electric dipole moment changes, which means that the optical transition frequencies of nearby ions change. If this dipole-dipole interaction is strong, it will cause a large detuning when an ion is excited and nearby ions will no longer be excited by light at their original resonance frequency—an effect known as dipole blockade. The strength of the interaction depends on the distance between the ions, as is discussed in Sec. II D.

A pulse resonant with the $|0\rangle \rightarrow |e\rangle$ transition of a control ion will thus change the local electric field surrounding the
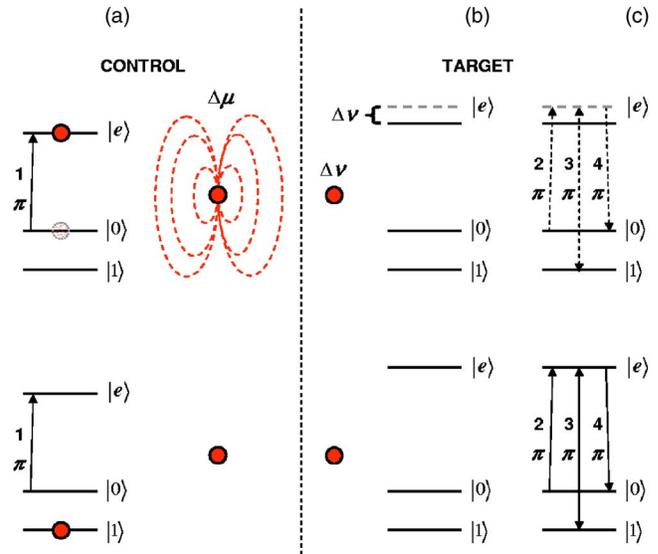
FIG. 3. (Color online) Schematic description of a controlled-NOT gate. (a, top) If the control qubit is originally in state $|0\rangle$, pulse 1 will transfer it to the excited state $|e\rangle$, and since the static dipole moment is different for the ground state and the excited state, the electric field in the vicinity of the ion changes. (b, top) This causes a Stark shift of optical resonance frequency of the neighboring ions. (c, top) Gate pulses on the original resonance frequencies of the target will no longer have any effect. A final pulse (not shown) transfers the control ion back to state $|e\rangle$. The lower part of the figure shows the effect of the same pulse sequence when the control qubit is originally in state $|1\rangle$. The first pulse will not be resonant with the ions, and the qubit NOT operation will be executed on the target qubit.

ion provided it was initially in state $|0\rangle$ [Fig. 3(a)]. If a target ion is situated close to the excited control ion, it will experience a Stark shift, changing its optical transition frequency ν if the control ion is excited, as in Fig. 3(b). Applying the three pulses shown in Fig. 3(c), the NOT operation will only be carried out if the control ion was originally, and still is, in state $|1\rangle$. With the control ion originally in state $|0\rangle$ the energy levels will be shifted, as depicted in the top part of Fig. 3(c). The three π pulses impinging on the target ion will be off resonance and the target ion will remain in its initial state. A final pulse on the $|e\rangle \rightarrow |0\rangle$ control ion transition, not shown in the figure, transfers the control ion down to the ground state if it was excited by the first pulse. Together, these pulses perform a CNOT operation.

As long as the ions are in their ground states the interaction can be disregarded. Note that, even though the magnitude of the Stark shift of the optical transition is unknown, this will never lead to phase accumulation for a qubit ion with sufficiently large shift, since the random shift only blocks the ion from being excited. The ions are only excited to the optically excited state if they have not experienced a shift and thus they will still have their original resonance frequency.

B. Optical pumping

The RE crystal ions are trapped in their lattice sites and they may be located very close to each other. They may still

have very good coherence properties—up to tens of seconds for the hyperfine levels [25] and up to 6.4 ms for the optical transition [11]. Ions located spatially very close, but belonging to different frequency groups, are addressed separately by selecting the appropriate transition frequency of the optical excitation pulses. However, there are several challenges which have to be met. As mentioned in Sec. I, it is difficult to read out a single ion. Having many instances of quantum computers running separately which can be read out in parallel gives a strong readout signal and offers a solution to this problem. However, initially there is a continuous distribution of ions all across the absorption profile. When optical pulses interact with ions at a specific qubit frequency, ions absorbing at nearby frequencies will also be affected by the radiation. This is solved by an optical pumping procedure, which isolates a group of ions spectrally and prepares them in a specific hyperfine (qubit) state. In this procedure, the spontaneous decay may be viewed as moving entropy from the sample to the surroundings.

The initial smooth distribution of the absorption over a large frequency range is depicted in Fig. 1(a). Over a limited frequency interval, the absorption will be essentially constant. A laser illuminating a certain frequency region will excite the ions within this interval. If these ions relax to their original hyperfine state, they will be excited again, until they end up in another hyperfine state, where they will remain for a long time since they are unaffected by the field. The laser is scanned back and forth across a small frequency interval and after a while a *pit* without any ions within the frequency interval is created; see Fig. 1(b). By repeating this procedure, with certain modifications as described in Ref. [27], one can lift back a subgroup of ions, all absorbing on a single hyperfine transition; see Fig. 1(c). This procedure can be repeated at different, well-separated frequencies, creating several qubits. Finally, for two-qubit gate operations ions which are not located close enough to interact strongly have to be removed. This is described in Sec. II D.

C. Population transfer using complex hyperbolic secant pulses

Each qubit consists of a group of ions which all have nearly the same resonance frequency. When viewed in the frequency domain, they are positioned in a pit where there are no other absorbing ions, as was described above. However, at frequencies outside the pit there are many ions. It is important that all ions in the peak experience the same pulse area during gate operations. At the same time, it is crucial not to excite ions outside the pit, since this would change the electric field near these ions, which could interfere with the operations. A good pulse should fulfill three criteria: It should have the same effect on all qubit ions, leave other ions (i.e., ions outside the pit) in the ground state, and be as short as possible to allow many gate operations within the coherence time [1,20]. In order to study the effect of different pulses on ions with slightly different resonance frequencies, the Bloch equations were solved numerically with the lifetime of the excited state set to $T_1 = 164$ μs, the laser coherence time set to 10 μs, and a maximal intensity corresponding to a Rabi frequency of $\Omega_{max} = 1$ MHz. A simple

Gaussian pulse, with an intensity width $t_{FWHM} = 0.33$ μs and a total truncated duration $t_{cutoff} = 2$ μs, can fulfill two of the criteria; it can be short and still leave the ions outside the pit unaffected [see Fig. 4(a)]. However, the excitation will not be uniform across the spectral width of the peak and, furthermore, the degree of excitation that a Gaussian pulse gives is sensitive to intensity variations. In NMR, the complex hyperbolic secant, sech, pulse has been investigated for use in similar situations [32]. The amplitude of the Rabi frequency of the sech pulse, $\Omega(t)$, is given by

$$\Omega(t) = \Omega_{max} \operatorname{sech}[\beta(t - t_0)], \qquad (1)$$

where β is related to the width of the pulse and Ω_{max} is the maximum Rabi frequency. The sech pulse has a tanh frequency chirp centred around frequency ν_c,

$$\nu = \nu_c + \frac{\mu\beta}{2\pi} \tanh[\beta(t - t_0)], \qquad (2)$$

where ν is the instantaneous frequency (Hz) and μ is a real constant. For convenience we will state some simple relations. Since $I \propto \Omega^2$, Eq. (1) can be rewritten as

$$I(t) = I_{max} \operatorname{sech}^2[\beta(t - t_0)], \qquad (3)$$

where I_{max} denotes the intensity which gives the Rabi frequency Ω_{max}. It is now easy to see that β relates to the full width half maximum of the intensity of the pulse, t_{FWHM}, as

$$t_{FWHM} = \frac{2}{\beta} \operatorname{arcsech} \sqrt{\frac{0.5 I_{max}}{I_{max}}} \approx \frac{1.76}{\beta}. \qquad (4)$$

This pulse will create a complete population inversion across a frequency interval ν_{width}, which is of the order of $2\mu\beta/2\pi$, as long as $\mu \geq 2$ and $\Omega_{max} \geq \mu\beta/2\pi$ (in Hz). Figures 4(b)–4(d) compare different implementations of sech pulses, for driving an optical transition with a finite excited state lifetime. In Fig. 4(b) the pulse parameters are those used for the three-state transfers discussed in Sec. IV B, which can be seen to create a theoretical inversion of 93%. The dashed (dashed red online) curve shows the analytically calculated inversion for an infinitely long sech pulse with no decoherence or decay calculated using the expression given by Silver *et al.* [32]. If the same parameters were used in the simulation, they gave identical results. In Fig. 4(c) the effects of a longer pulse are shown. A longer pulse can give sharper inversion edges, but due to the limited coherence time of the laser the inversion is lower ($\sim 85\%$). Figure 4(d) shows the effect of the truncation (cutoff). The values of t_{FWHM} and ν_{width} are the same as in Fig. 4(b) but t_{cutoff} was changed from 3 to 2.5 μs. Even though the effect on the intensity profile of the pulse is hardly noticeable, the effect on the transferred population is striking. If the coherence time is increased to 100 μs and a long pulse is used, a population transfer efficiency of $\sim 98\%$ can be achieved, as shown in Fig. 4(e). Furthermore, above a threshold value, the sech inversion is insensitive to field intensity variations which is an important experimental advantage. A complete CNOT operation can be performed using sech pulses. The complete pulse sequence for the CNOT gate has been studied theoretically and numerically simulated [1], including effects of superposition input
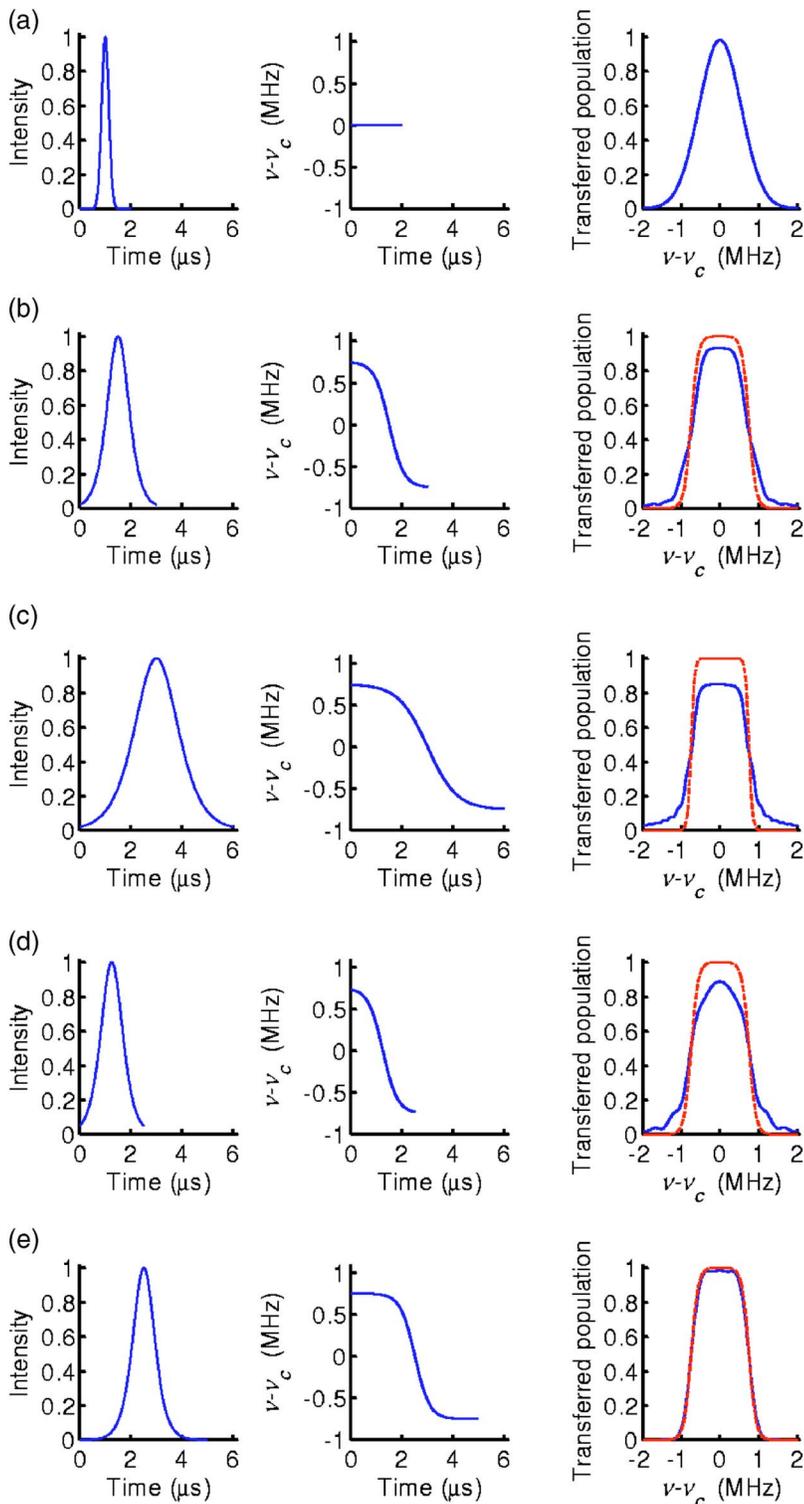
FIG. 4. (Color online) Theoretical calculations of population transfer using optical pulses. The left column shows the intensity envelope of the pulses, the middle column shows the instantaneous frequency of the pulse, and the right column shows the simulated, solid line (blue online), and analytically calculated, dashed line (dashed red online), transfer for the same pulse. In simulations (a)–(d) a laser coherence time of 10 μs is used. All pulse lengths are given as the intensity FWHM. (a) Transfer using a Gaussian pulse with $t_{FWHM}=0.33$ μs and $t_{cutoff}=2$ μs gives effective transfer for a narrow frequency interval since it is short and therefore less sensitive to decoherence. But only a small change, decrease or increase, in intensity will make the transfer much less effective. (b) Transfer using a sech pulse, $t_{FWHM}=1$ μs, $t_{cutoff}=3$ μs, and $\nu_{width}=1.5$ MHz gives a transfer efficiency of ~93%. These pulse settings were used for the three-state transfer experiments shown in Figs. 9 and 10. (c) Transfer using a sech pulse, $t_{FWHM}=2$ μs, $t_{cutoff}=6$ μs, and $\nu_{width}=1.5$ MHz yields an efficiency of ~85%. A longer pulse makes the inversion flatter but smaller due to larger susceptibility to decoherence. This pulse was used for the two-level transfer experiments shown in Fig. 8(g). (d) Sech transfer with $t_{FWHM}=1$ μs, $t_{cutoff}=2.5$ μs, and $\nu_{width}=1.5$ MHz. Even though the change in cutoff from case (b) is barely visible in the intensity plot, the effect is evident in the population transfer. (e) If the coherence time is increased to 100 μs the transfer efficiency is predicted to be 98%, $t_{cutoff}=5$ μs and $\nu_{width}=1.5$ MHz.

states and compensation of phase due to the slight variations in transition frequency within the qubits.

D. Selecting only the strongly interacting ions

For ions separated by some distance r, the dipole-dipole interaction used for two-qubit gates is proportional to $1/r^3$. Since the ions are randomly located in the sample, ions absorbing within a given frequency interval will interact to varying degrees with any other set of ions, depending on their relative positions. When a set of ions in the material, absorbing at some given frequency ν_1 is excited, other ions that were originally absorbing at some other frequency ν_2 will be shifted by various amounts, leading to a broadening, known as instantaneous spectral diffusion. The dephasing caused by the random frequency shifts is called excitation-induced dephasing and can be studied in experiments with

$\lambda_{vac}\left[{}^1D_2(1)\rightarrow{}^3H_4(1)\right]$	605.977 nm
Γ_{hom}	970 Hz
Γ_{inhom}	~5 GHz
T_1	164 µs
T_2	152 µs
T_h (Hole lifetime)	~100 s
α	20 cm^{-1}
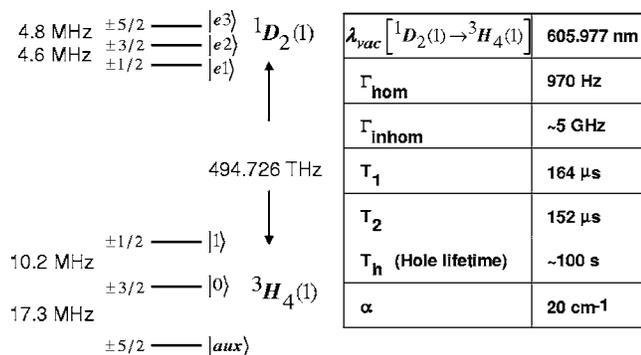
FIG. 5. Summary of relevant data for the ${}^3H_4 \rightarrow {}^1D_2$ transition of site I in Pr^{3+}:Y_2SiO_5 and state labels used throughout this paper. T_1, T_2, and Γ_{hom} are given according to Ref. [42].

coherent transients [33,34]. These inherently unordered inter-action processes are detrimental to many applications, but by choosing to use only a selected subset of ions, with strong interactions, we can use them in a structured manner for controlled operations.

To describe the procedure for choosing only qubit ions located close to ions belonging to each of the other qubits and therefore having strong interactions with them, we consider one target and one control qubit. A third ground-state hyperfine level denoted $|aux\rangle$ (Fig. 5) can be used for storing ions with too weak interactions. For the group of ions in the target qubit, excitation of the control ion qubit shows up as a broadening of the absorbing target peak [15]. Figure 6(a) shows the peak before any control ions have been excited, and Figs. 6(b)–6(d) show the broadening caused by exciting control intervals with increasing frequency widths—i.e., with increasing density of excited ions. Figure 6(e) shows the re-assembled peak after the control ions have returned to the ground state. The ions that can be used for gate operations are those which interact strongly with the control qubit—i.e.,
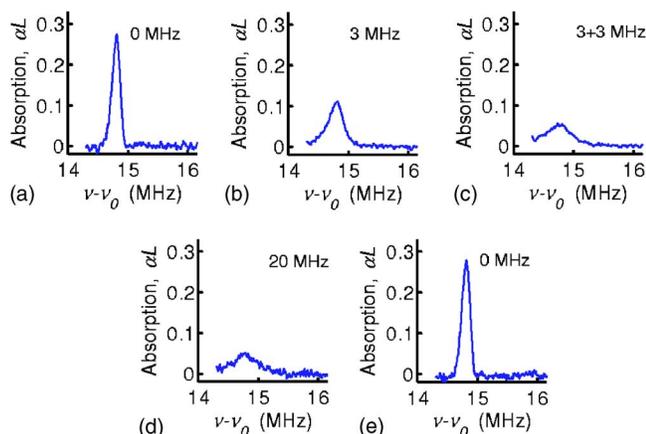
FIG. 6. (Color online) Shift of the resonance frequency of ions due to changes in local electric fields caused by the excitation of nearby ions, absorbing at a different frequency. (a) The peak before excitation. (b), (c), and (d) Exciting 3-, 6-, and 20-MHz intervals, respectively, corresponding to an increasing density of excited ions. (e) The control ions have returned to the ground state and the peak regains its initial shape. Single-shot data.
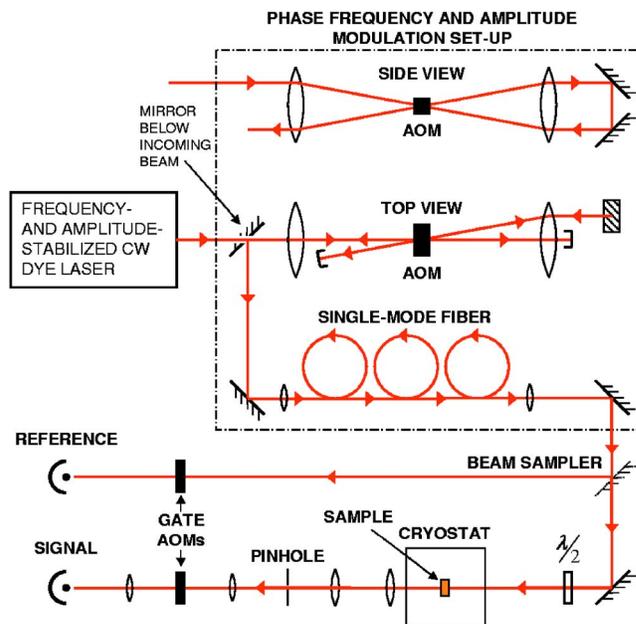
FIG. 7. (Color online) Setup used in the experiments. See the text, Sec. III, for details.

the ions that experience a large change in resonance frequency in response to the control ion excitation. The ions that undergo a small shift can be removed from the qubit after control ion excitation by selectively promoting them to the upper state using, e.g., sech pulses such as those described in Sec. II C. The control ions are then returned to their ground state with a third pulse. The weakly interacting and now excited target ions are then allowed to decay to the ground state. Since they do not all decay to the $|aux\rangle$ state, the procedure has to be repeated several times, until all ions with insufficient interactions have been removed from the qubit peak, as is further discussed in Sec. V.

III. EXPERIMENTAL SETUP

The experimental setup is depicted in Fig. 7. An 8-W, Coherent Verdi-V8, 532-nm Nd:YVO$_4$ laser pumps a Coherent 699-21 dye laser emitting approximately 300 mW of laser light at 605.977 nm. The linewidth of the commercially available dye laser system is ~1 MHz, which is too broad for the present experiments. Therefore, the laser frequency error was measured against a vacuum-suspended high-finesse cavity, with a free spectral range of 530 MHz and 1 MHz linewidth, using the Pound-Drever-Hall technique [35]. This error signal was then fed back to an intracavity electro-optical modulator (LINOS PM25) in the laser cavity. This decreased the laser's linewidth to ~30 kHz. The amplitude fluctuations of the dye laser were suppressed with an external acousto-optic modulator (AOM) after the dye laser.

The light then entered the modulator setup, which created light pulses with arbitrarily chosen phase, amplitude, and frequency patterns with high definition, even at low amplitudes. It consisted of an acousto-optic modulator (AA opto-electronic model AA.ST.200/B100/A0.5-vis) through which the light passed twice. If the position of this AOM is adjusted

precisely along the beam direction, the light frequency can be shifted without any spatial displacement of the output beam. A bow tie configuration was used to avoid back reflection into the laser; see Fig. 7. The radio frequency signal used to drive the AOM was created with a 1-GS/s 10-bit arbitrary wave form generator (Tektronix AWG520). The generator was programmed from a PC where a Labview/Matlab software generated and downloaded the pulse sequences to the generator. The output signal from the generator was attenuated by 10 dB, to avoid component damage, and then amplified by a 50-W amplifier (Mini-Circuits, LZY-1). The amplifier was overdimensioned in order to minimize nonlinear distortion effects, and the radio frequency signal was finally attenuated by 3 dB, to minimize cable reflection effects, before being fed to the AOM. After the AOM the light was passed through a single-mode fiber, to clean up the spatial mode. The AOM, together with the fiber, created a beam with good mode quality and no beam walk, which could be modulated arbitrarily over 200 MHz, with a total transmission that did not fall below 25% anywhere within the frequency range. The smooth variation in efficiency as a function of frequency and the nonlinear amplitude response of the setup were measured and compensated for, when the different wave forms were calculated.

Five percent of the light was split off by a beam sampler (Thorlabs, BSF10-A1) after the fiber and used as a reference. The rest of the light was passed through a $\lambda/2$ plate and was focused onto the sample with a $f=300$ mm lens, which yielded a $1/e^2$ spot diameter of ~ 100 μm throughout the sample. The intensity at the sample was ~ 20 mW, which gave a Rabi frequency of ~ 1 MHz for the stronger transitions. This was the Rabi frequency used for all the sech transfer experiment unless otherwise stated.

The sample was mounted in vacuum inside a continuous helium flow cryostat and was kept at ~ 3.5 K. The sample consisted of a 0.5-mm-thick Y_2SiO_5 crystal where 0.05% of the Y ions had been substituted by Pr^{3+}. The crystal was oriented so that the b axis was parallel to the direction of propagation of the light. The $\lambda/2$ plate was rotated to obtain maximum absorption. This was assumed to be when the electric-field projection onto the transition dipole moment was the same for the two different orientations of the Pr^{3+} in site 1. Figure 5 shows the energy level diagram and a summary of some important data for the material.

The light transmitted through the crystal was imaged onto a 50-μm pinhole with a magnification ratio of 1.15. The pinhole only transmits light from the center of the laser spot in the sample; within this region the intensity varied by less than 20%. Both the reference and the signal beam were gated by AOM's before being detected by two matched detectors (own design, rise time 3 μs, transimpedance 330 kΩ). The signals from the two detectors were recorded on an oscilloscope (Tektronix, TDS 540) and transferred to the computer and software that programmed the arbitrary wave form generator. The software divided the two signals to reduce the effect of laser amplitude fluctuations.

Four different types of pulse were used in the experiments.

(i) The first type was 100–500-ms-long series of incoherent pulses, which were used to create peaks of ions, where all
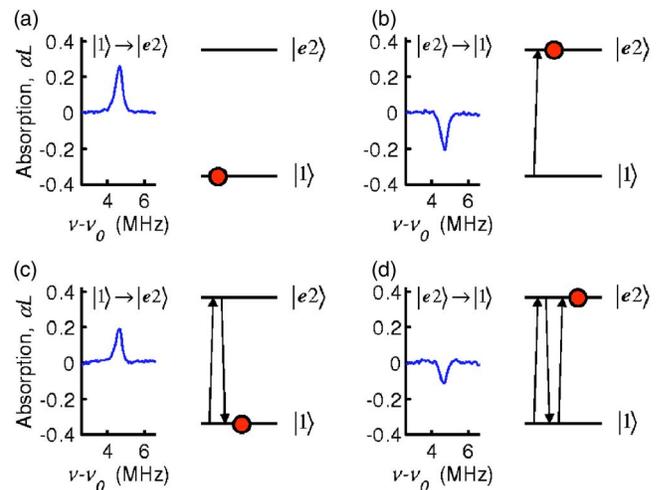
FIG. 8. (Color online) Population transfer between the ground and optically excited states. (a) The qubit starts in state $|1\rangle$. (b) Applying one sech pulse to the $|1\rangle \rightarrow |e2\rangle$ transition transfers the qubit to state $|e2\rangle$. (c). Another sech pulse transfers the qubit back to state $|1\rangle$. (d) A third sech pulse will again transfer the qubit to state $|e2\rangle$. Single-shot data.

the ions were in a specific hyperfine level [27].

(ii) The second type was short coherent pulses, mainly complex sech pulses, which robustly and effectively transferred population between different levels.

(iii) The third pulse type was a modification of the sech pulse, where the center of the pulse, in both amplitude and frequency, was extended with a straight line. This was used to invert larger frequency regions than was possible with the sech pulse. We call this pulse type a sech scan. At the time of the experiments the authors were not aware of the more sophisticated pulses developed for such a purpose [36,37].

(iv) The fourth type of pulses was used to measure the number of ions in the different states. To that end the laser frequency was scanned across the absorption profile, while monitoring the absorption.

In principle the frequency scan can be arbitrarily fast. By calculating the spectral content of the readout field and the transmitted light [38–40], the original absorption profile can be computed [41]. These experiments were, however, carried out in the slow passage regime, where the measured transmission signal is proportional to the absorption and the frequency resolution Δv is limited by the readout frequency chirp rate r, $\Delta v \propto \sqrt{r}$. Using the method of scanned readout gives some artifacts. Ions in an excited state will have time to decay during the readout scan. This means that the upper-state population can be smaller near the end of the scan than at the beginning of the scan. It is therefore a good idea, especially when probing inverted populations, to put the frequency corresponding to the transition of interest as close to the beginning of the readout scan as possible. If the intensity of the readout pulse is too high, the readout pulse will itself alter the populations. For these two reasons, fast readout may be favorable, although this can lead to ringing after sudden changes in absorption [41], which can sometimes make the absorption appear to be below 0%. Balancing the readout-induced excitation against the signal-to-noise ratio yielded
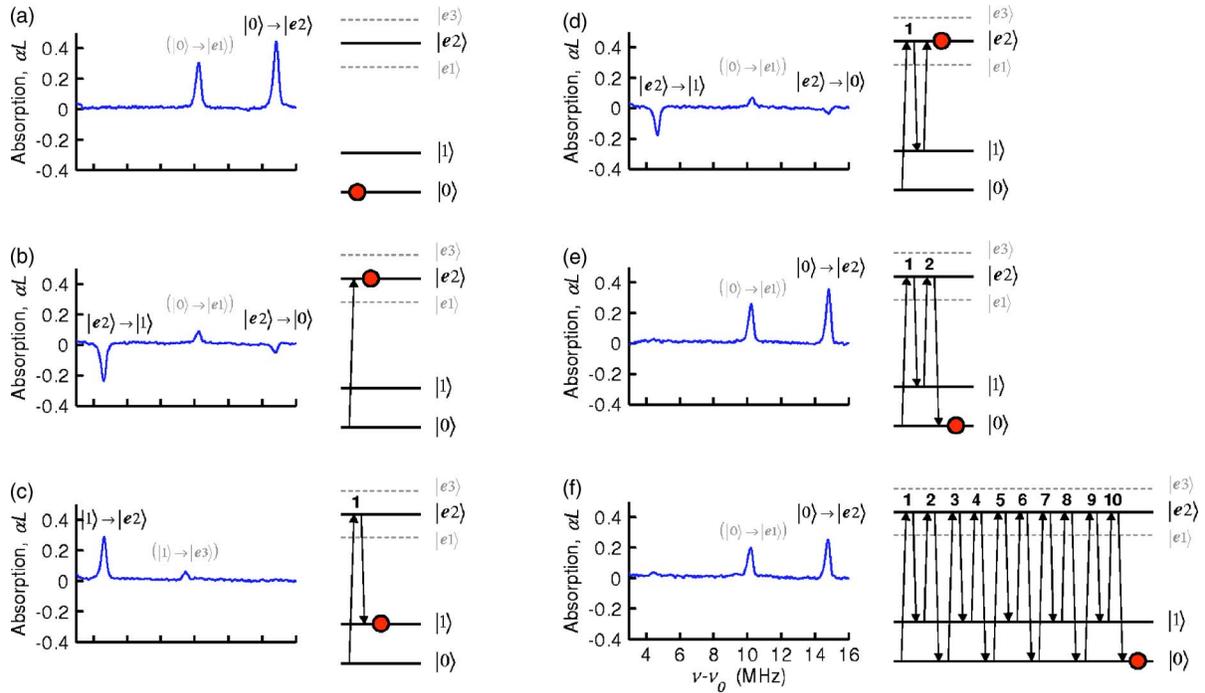
FIG. 9. (Color online) Multiple population transfer between two ground state levels via an excited state. The graphs on the left show the absorption during readout scans after completion of the operation, while the energy diagrams on the right schematically show the state of the qubit. Peaks in parentheses are the same ions absorbing to different excited levels. (a) The qubit is originally in state $|0\rangle$. (b) The qubit is transferred to state $|e2\rangle$ with a sech pulse resonant with the $|0\rangle \rightarrow |e2\rangle$ transition, which causes strong stimulated emission on the $|e2\rangle \rightarrow |1\rangle$ transition at the beginning of the scan. During the readout scan (130 μs) the qubit partly relaxes back to the ground state and therefore absorption on the transition $|0\rangle \rightarrow |e1\rangle$ can be seen in the middle of the scan and the $|e2\rangle \rightarrow |0\rangle$ inversion at the end of the scan is small. (c) A second sech pulse brings the qubit down to state $|1\rangle$. (d) A third sech pulse transfers the qubit to the state $|e2\rangle$, (e) followed by a fourth sech pulse, transferring the qubit back to $|0\rangle$. (f) Ten complete ground state-to-ground state transfers, each caused by two sech pulses. Single-shot data.

readout intensities typically ranging between 10^{-3} and 10^{-4} times the intensities used in the population transfer pulses. The noise floor in the different data recordings depends on the readout intensity used in that particular experiment.

IV. EFFICIENT AND ROBUST POPULATION TRANSFER WITH SECH PULSES

In this section, experimental results confirming that the sech pulses proposed in Ref. [1] are highly efficient for selective transfer of qubits defined in the frequency domain are presented. Although some of these state-to-state transfers may seem quite trivial, the pulse sequences required to obtain the data are actually quite elaborate. For example, creating the zero-absorbing background, the target and control qubits and the distillation operations in Fig. 11(d) requires 305 frequency-chirped pulses. However, in practice it is just a question of programming the arbitrary wave form generator used to drive the AOM's carrying out the task.

A. Two-state transfer

Transferring a qubit from state $|1\rangle$ to an optically excited state $|e2\rangle$ is a basic qubit operation. Figure 8(a) shows the absorption by a qubit in state $|1\rangle$ on the $|1\rangle \rightarrow |e2\rangle$ transition

during a weak readout scan. Applying one sech pulse with its center frequency at the $|1\rangle \rightarrow |e2\rangle$ transition transfers the qubit to the optically excited state $|e2\rangle$. The readout scan in Fig. 8(b) shows the stimulated emission from the qubit after the transfer. When two sech pulses are applied directly after each other the qubit will be transferred to state $|e2\rangle$ and then back again to state $|1\rangle$, as shown in Fig. 8(c). Finally, three consecutive pulses will leave the qubit in state $|e2\rangle$, as seen in Fig. 8(d). As the qubit is transferred up and down an increasing number of ions will be lost, mainly due to decoherence. (The coherence time of the laser is ~ 10 μs.) The transition time for the ions during each sech pulse is approximately 2 μs, and during this time the ions accumulate errors. A second source of errors is that, although care was taken to have a uniform intensity all across the measured part of the focal spot, this was not fully achieved. Light from ions in the parts of the focus where the intensity is considerably lower and where the pulses were therefore inefficient will leak though and be detected. Variations in the apparent transfer efficiency in these experiments can, to a large degree, be explained by misalignment of the detection pinhole. Even though sech transfer is robust against intensity variations, this is only true above the threshold. If the pinhole is slightly misaligned, some of the detected light will come from the areas with much lower intensity, where the sech pulses do not work properly, and the transfer efficiency is therefore
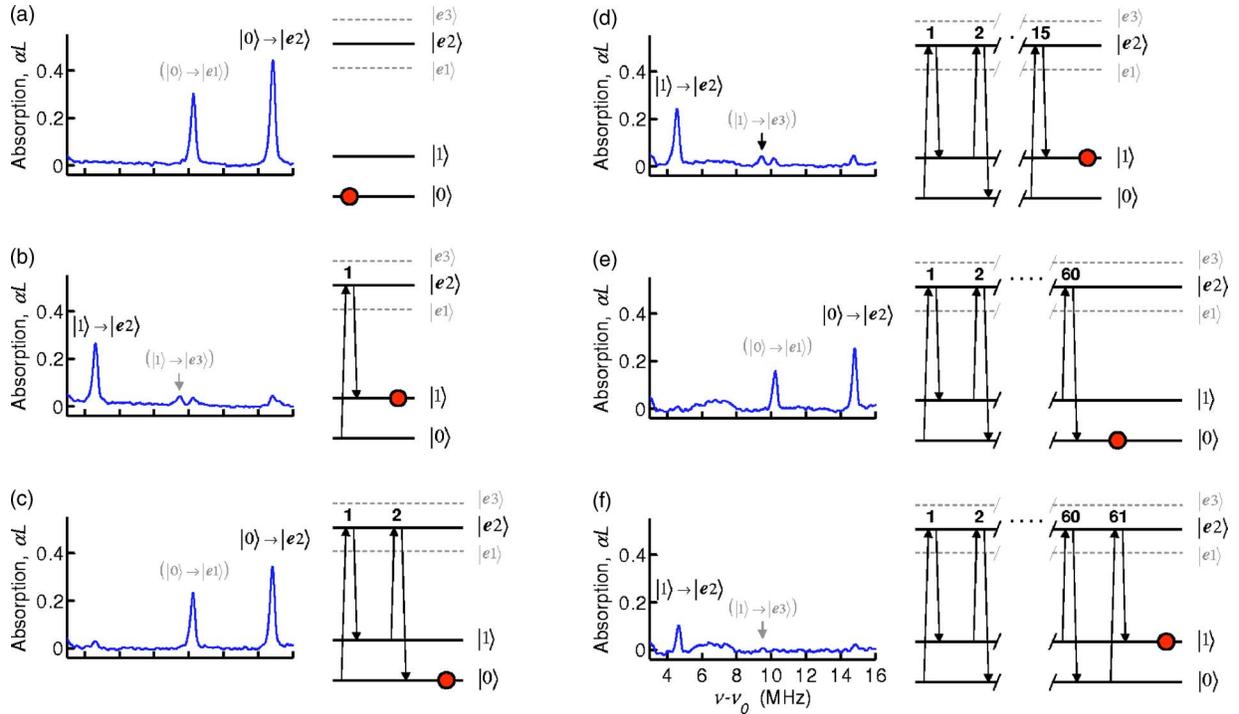
FIG. 10. (Color online) Repeated population transfer between ground-state sublevels via an excited state, with a 500-μs delay between each transfer. The graphs on the left show the readout scan 500 μs after completion of the operation. The energy diagrams on the right schematically show the state of the qubit. The peaks in parentheses are the same ions absorbing to different excited levels. (a) The qubit is originally in state $|0\rangle$. (b) The qubit has been transferred to state $|1\rangle$ using two sech pulses, resonant with the $|0\rangle \rightarrow |e2\rangle$ and $|e2\rangle \rightarrow |1\rangle$ transitions, respectively. (c) The qubit has been transferred back to state $|0\rangle$. (d) Fifteen transfers. (e) Sixty transfers between the two ground-state sublevels. (e) Sixty-one transfers. Single-shot data.

strongly reduced. The third source of error comes from the limited lifetime of the excited state, 164 μs [42].

B. Three-state transfer

By driving two connected optical transitions, ions can be transferred between two sublevels of the ground state—e.g., two qubit states. Since the two optical transitions have different transitions frequencies, a pit with no absorbing ions also has to be cleared around the new frequency. In $Pr^{3+}:Y_2SiO_5$ it was possible to clear a pit which, for one qubit, will accommodate the transitions from states $|0\rangle$ and $|1\rangle$ to the same excited state [27], in this case state $|e2\rangle$. Figure 9(a) shows a qubit in state $|0\rangle$ absorbing to state $|e2\rangle$. Transitions to this excited state will be used to transfer the qubit between states $|0\rangle$ and $|1\rangle$. Peaks that correspond to qubit absorption on transitions other than those used for qubit transfer are given in parentheses in the figures—e.g., the second peak from the right in Fig. 9(a), which corresponds to transition $|0\rangle \rightarrow |e1\rangle$. In Fig. 9(b), the qubit has been transferred with a sech pulse from state $|0\rangle$ to state $|e2\rangle$ and stimulated emission from transition $|e2\rangle \rightarrow |1\rangle$ can be seen at the beginning of the scan. One might expect a similar amount of stimulated emission from the peak corresponding to the transition $|e2\rangle \rightarrow |0\rangle$ at the end of the scan. The reason for the difference in size is the decay to the ground states during the 100 μs it takes for the readout scan to pass across the two peaks. The small peak in the middle of the graph arises from

the ions that decayed back to state $|0\rangle$ during the readout scan. If a second sech pulse resonant with the $|e2\rangle \rightarrow |1\rangle$ transition directly follows the first pulse, this will transfer the population down to state $|1\rangle$, as can be seen in Fig. 9(c). When many pulses are applied in immediate succession the qubit can be moved back and forth between states $|0\rangle$ and $|1\rangle$ via state $|e2\rangle$ as is shown in Figs. 9(d)–9(f). Note that decay between the sech pulses is small, as the pulse separation is only 3 μs.

By incorporating a delay of 500 μs between transfer between states, any population left in the excited state due to incomplete transfer will be given time to relax. Once the qubit has been transferred from one ground state to the other, it can reside there for a long time. The transfer was repeated up to 61 times, as shown in Figs. 10(a)–10(f), where the readout also was also delayed by 500 μs after the last operation.

V. QUBIT DISTILLATION

The procedure of selecting only ions with sufficient qubit-qubit interaction is referred to as qubit distillation. Selected target ions should experience a large enough frequency shift when the control qubit is excited in order for the dipole blockade effect to work. The experimental results regarding qubit distillation are shown in Fig. 11. First the control ions are excited, which induces a large frequency shift of the optical resonance frequency in target ions that are close to
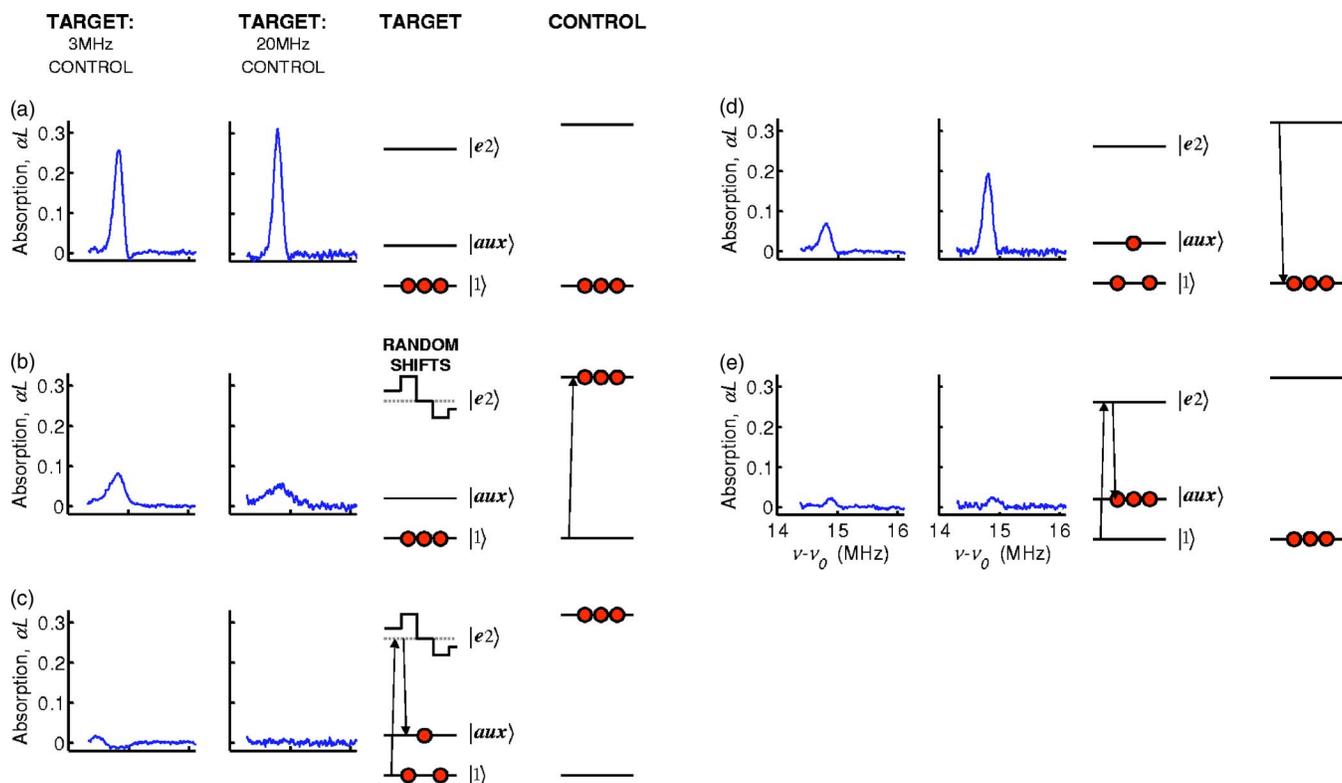
FIG. 11. (Color online) Selecting target ions that interact strongly with the control ions. The leftmost column shows data using a 3-MHz control interval and the next column using a 20-MHz control interval. The third and fourth columns schematically depict the state of the target and control ions, respectively. (a) The original peak consists of both controllable and noncontrollable ions. (b) Exciting the control ions shifts the resonance frequencies of the strongly interacting ions. (c) The ions that do not shift are transferred to state $|aux\rangle$, using two sech pulses. (d) After the control ions have relaxed back to the ground state, the controlled ions return to their original resonance frequencies. (e) If the two sech pulses used in (c) are used to remove the peak of ions without first exciting the control ions, almost all of the peak is removed. The difference between (d) and (e) shows the efficiency of the selection. Single-shot data.

one of the ions belonging to the control qubit. A sech pulse then transfers the ions remaining near their original optical resonance frequency to the optically excited state, and a second sech pulse then transfers them to the auxiliary state. Finally, the control ions return to their ground state.

The distillation procedure was investigated using two different sets of control ions, first using control ions absorbing within a 3-MHz interval and then using ions absorbing within a 20-MHz interval. Since there are more control ions in the latter case, we expect more target ions to be close to a control ion. Figure 11 has four columns, of which the first and second show target data for control intervals of 3 and 20 MHz, respectively. The third and fourth columns show the conceptual state of the target and control ions, respectively. Figure 11(a) shows the conditions before distillation. The two peaks differ in size because of the slightly different sech pulse parameters used to create them. In Fig. 11(b) the control interval has been excited. No pulses have yet been applied to the target ions, but they appear broader and lower because the resonance frequency of the ions has changed. The two sech pulses that remove the unshifted ions are then applied, and Fig. 11(c) shows the situation after these pulses, but with the control ions still excited. In Fig. 11(d) the control ions have relaxed back to the ground state. The target

ions which experienced a large shift, and were therefore unaffected by the removing sech pulses, have now returned to their original resonance frequency. Ideally, the remaining peak should be the strongly interacting ions. Figure 11(e) shows the situation when the sech pulses have been applied without first exciting the control qubit. Ideally, all the target ions should have been removed in this case. The difference between Figs. 11(d) and 11(e) shows how well the qubit was distilled in the present experiments. Approximately 85% of the remaining ions in the 20-MHz case were controlled by the excited ions. The distillation efficiency was mainly limited by the laser coherence time. By repeating the procedure, it should be possible to reduce the number of weakly interacting ions further. This can only be done for an interval which is smaller than the separation between the excited states, ~3 MHz, as the pulse used to transfer the control ions would otherwise interact with the same ions several times. We used two sech pulses to transfer the weakly interacting ions to the auxiliary state, which in this experiment was actually state $|0\rangle$. In future experiments the weakly interacting ions will instead be pumped to state $|e3\rangle$ from where they mainly relax to the normal state $|aux\rangle$, as the branching ratio for this transition is close to unity [27].

VI. SUMMARY AND OUTLOOK

In a rare-earth-metal-ion-doped crystal at liquid helium temperatures the $4f$-$4f$ transitions of individual ions can have sub-kHz linewidths, but inhomogeneous broadening of these transitions leads to GHz-wide line profiles. The line profiles can be tailored using optical pumping to isolate a frequency group of ions leading to a situation in part resembling the situation for laser-cooled atoms or ions or single-molecule spectroscopy. In this work it was demonstrated how the homogeneous transitions can then be investigated and atoms moved efficiently from state to state using optical pulses, without affecting ions absorbing at other frequencies. These techniques for isolating groups of ions in rare-earth-metal solids can be particularly interesting since the $4f$-$4f$ transitions of some of these optical rare-earth metals are claimed to be the most narrow transitions observed in solids [11].

The complex hyperbolic secant pulses, proposed by Roos and Mølmer [1] to be efficient for state-to-state transfer of selected frequency groups of ions, were shown to indeed provide very robust transfer. That sech pulses are effective for frequency-selective transfer is also supported by the work by Crozatier *et al.* on a two-level system in Tm:YAG [18]. In our work many consecutive state-to-state transfers were carried out. The deviation from 100% efficiency can mainly be explained by the dephasing caused by the 30-kHz laser linewidth during the state-to-state transfer. The laser linewidth is almost an order of magnitude larger than the homogeneous transition linewidth for the ions. Thus there is reason to believe that the transfer efficiency in our Pr:YSO crystal can be improved significantly.

The RE crystal dopant ions are located at random positions in the crystal. Using optical pumping and ion frequency selection with the sech pulses, an ensemble of target ions was selected where up to 85% are located spatially close to an excited control ion [Fig. 11(d)]. In this way an organized and ordered interaction can be obtained with the ions in the crystal although it is randomly doped. The extremely narrow transition lines actually enable us to select ions pairs with very specific interaction strengths. Finally, looking to the future, we feel that the efficient state-to-state transfer and distillation results now put the two-bit gate operation in RE crystals well within reach.

[1] I. Roos and K. Molmer, Phys. Rev. A **69**, 022321 (2004).

[2] id Quantique, http://www.idquantique.com

[3] magiQ, http://www.magiqtech.com

[4] Los Alamos National Laboratory, http://qist.lanl.gov

[5] E. Knill, R. Laflamme, R. Martinez, and C. H. Tseng, Nature (London) **404**, 368 (2000).

[6] F. Schmidt-Kaler, H. Haffner, M. Riebe, S. Gulde, G. P. T. Lancaster, T. Deuschle, C. Becher, C. F. Roos, J. Eschner, and R. Blatt, Nature (London) **422**, 408 (2003).

[7] X. Q. Li, Y. W. Wu, D. Steel, D. Gammon, T. H. Stievater, D. S. Katzer, D. Park, C. Piermarocchi, and L. J. Sham, Science **301**, 809 (2003).

[8] J. J. Longdell, M. J. Sellars, and N. B. Manson, Phys. Rev. Lett. **93**, 130503 (2004).

[9] V. Lavielle, F. de Seze, I. Lorgere, and J. L. Le Gouet, J. Lumin. **107**, 75 (2004).

[10] K. D. Merkel, R. K. Mohan, Z. Cole, T. Chang, A. Olson, and W. R. Babbitt, J. Lumin. **107**, 62 (2004).

[11] Y. Sun, C. W. Thiel, R. L. Cone, R. W. Equall, and R. L. Hutcheson, J. Lumin. **98**, 281 (2002).

[12] N. Ohlsson, R. K. Mohan, and S. Kröll, Opt. Commun. **201**, 71 (2002).

[13] K. Ichimura, Opt. Commun. **199**, 453 (2001).

[14] M. D. Lukin and P. R. Hemmer, Phys. Rev. Lett. **84**, 2818 (2000).

[15] M. Nilsson, L. Rippe, N. Ohlsson, T. Christiansson, and S. Kröll, Phys. Scr. **T102**, 178 (2002).

[16] M. J. Sellars, E. Fraval, and J. J. Longdell, J. Lumin. **107**, 150 (2004).

[17] J. J. Longdell and M. J. Sellars, Phys. Rev. A **69**, 032307 (2004).

[18] V. Crozatier, F. de Seze, L. Haals, F. Bretenaker, I. Lorgeré, and J. L. Le Gouet, Opt. Commun. **241**, 203 (2004).

[19] J. Wesenberg and K. Molmer, Phys. Rev. A **68**, 012320 (2003).

[20] J. H. Wesenberg, *Quantum Information processing in Rare-Earth-Ion-Doped Crystals* (University of Aarhus, Aarhus, 2004).

[21] N. Ohlsson, *Quantum Optics and Quantum Information Processing in Rare-Earth-Ion-Doped Crystals* (Lund Institute of Technology, Lund, 2002).

[22] J. H. Wesenberg, Phys. Rev. A **69**, 042323 (2004).

[23] P. Goldner and O. Guillot-Noel, Mol. Phys. **102**, 1185 (2004).

[24] M. Tian, Z. W. Barber, J. A. Fischer, and W. Randall Babbitt, Phys. Rev. A **69**, 050301(R) (2004).

[25] E. Fraval, M. J. Sellars, and J. J. Longdell, e-print quant-ph/0412061.

[26] Y. V. Malyukin, A. A. Masalov, and P. N. Zhmurin, Phys. Lett. A **316**, 147 (2003).

[27] M. Nilsson, L. Rippe, S. Kröll, R. Klieber, and D. Suter, Phys. Rev. B **70**, 214116 (2004).

[28] G. J. Pryde, M. J. Sellars, and N. B. Manson, Phys. Rev. Lett. **84**, 1152 (2000).

[29] M. Nilsson and S. Kröll, Opt. Commun. **247**, 393 (2005).

[30] A. A. Kaplyanskii, J. Lumin. **100**, 21 (2002).

[31] R. M. Shelby and R. M. Macfarlane, Opt. Commun. **27**, 399 (1978).

[32] M. S. Silver, R. I. Joseph, and D. I. Hoult, Phys. Rev. A **31**,

2753 (1985).

[33] M. Mitsunaga, T. Takagahara, R. Yano, and N. Uesugi, Phys. Rev. Lett. **68**, 3216 (1992).

[34] F. R. Graf, A. Renn, G. Zumofen, and U. P. Wild, Phys. Rev. B **58**, 5462 (1998).

[35] R. W. P. Drever, J. L. Hall, F. V. Kowalski, J. Hough, G. M. Ford, A. J. Munley, and H. Ward, Appl. Phys. B: Photophys. Laser Chem. **31**, 97 (1983).

[36] K. E. Cano, M. A. Smith, and A. J. Shaka, J. Magn. Reson. **155**, 131 (2002).

[37] E. Kupce and R. Freeman, J. Magn. Reson., Ser. A **115**, 273 (1995).

[38] J. E. Chin and C. E. Cook, Sperry Eng. Rev. **12**, 11 (1959).

[39] C. E. Cook, Proc. Inst. Radio Eng. **48**, 310 (1960).

[40] J. R. Klauder, A. C. Price, S. Darlington, and W. J. Albersheim, Bell Syst. Tech. J. **39**, 745 (1960).

[41] V. V. Khodos, D. A. Ryndyk, and V. L. Vaks, Eur. Phys. J.: Appl. Phys. **25**, 203 (2004).

[42] R. W. Equall, R. L. Cone, and R. M. Macfarlane, Phys. Rev. B **52**, 3963 (1995).